

## Article

# Long Distance Military Fiber-Optic Polarization Sensor Improved by an Optical Amplifier

Martin Kyselak <sup>1,\*</sup>, Jiri Vavra <sup>1</sup>, Karel Slavicek <sup>2</sup>, David Grenar <sup>3</sup> and Lucie Hudcova <sup>4</sup>

<sup>1</sup> Department of Electrical Engineering, Faculty of Military Technology, University of Defence Brno, 66210 Brno, Czech Republic

<sup>2</sup> IT Infrastructure Division, Institute of Computer Science, Masaryk University, 60177 Brno, Czech Republic

<sup>3</sup> Department of Telecommunications, Faculty of Electrical Engineering and Communication, Brno University of Technology, 60190 Brno, Czech Republic

<sup>4</sup> Department of Radio Electronics, Faculty of Electrical Engineering and Communication, Brno University of Technology, 60190 Brno, Czech Republic

\* Correspondence: martin.kyselak@unob.cz; Tel.: +420-724-692-581

**Abstract:** The ever-increasing demands for the use of fiber-optic sensors powered by long optical fibers is forcing developers to solve problems associated with powering these remote sensors. Due to their non-electric character, these sensors are suitable for many uses, including military applications. The Army of the Czech Republic is very interested in this type of optical fiber sensor as it fulfils the significant prerequisites for use in military areas. However, the army's requirements are challenging because they require long supply cables in which there is significant attenuation of optical power. At the same time, there is a need for high sensitivity. The subject of our research team's work was to use amplifiers to power these sensors. The army already uses this type of sensor for short distances as it cannot ignite a gas mixture with an explosive concentration and thus meet the strict requirements of the explosion-proof standard. The novelty of our research lies in the discovered measurement technique that allows the sensors to be powered remotely and in the saving of optical fibers by utilizing duplex communication with a circulator. Furthermore, the research presents an innovative approach to the optimization of the entire sensor by using a bidirectional, sensory, polarization-maintaining optical fiber. The proposed sensor was first verified in laboratory conditions at the Optoelectronics Laboratory of the University of Defense in Brno, and further tests were carried out in the military training areas of Boletice and Březina in the Czech Republic, which is a member of North Atlantic Treaty Organization.

**Keywords:** polarization sensor; birefringence; temperature sensor; military area; EDFA amplifier; wavelength multiplex



**Citation:** Kyselak, M.; Vavra, J.; Slavicek, K.; Grenar, D.; Hudcova, L. Long Distance Military Fiber-Optic Polarization Sensor Improved by an Optical Amplifier. *Electronics* **2023**, *12*, 1740. <https://doi.org/10.3390/electronics12071740>

Academic Editor: Nakkeeran Kaliyaperumal

Received: 28 February 2023

Revised: 27 March 2023

Accepted: 2 April 2023

Published: 6 April 2023



**Copyright:** © 2023 by the authors. Licensee MDPI, Basel, Switzerland. This article is an open access article distributed under the terms and conditions of the Creative Commons Attribution (CC BY) license (<https://creativecommons.org/licenses/by/4.0/>).

## 1. Introduction

The principle of fiber-optic polarization sensors is based on the physical properties of polarization-maintaining fibers that maintain the orthogonality of two optical waves propagating at different speeds. This difference in propagation speed is due to the birefringent properties of the optical fiber. The change in the polarization state is ultimately a parameter that is detected and further processed by the receiver [1,2]. Although this principle is known, it has its imperfections, which are addressed in this work. The first problem lies in the excitation of the optical fiber as it is necessary to excite both axes of the optical fiber with the same or comparable power. If this condition is met even when using considerably long optical paths (in the order of kilometers), the sensors will be able to be powered inside large areas with a risk of explosion. The second problem is the attempt to use existing telecommunications routes to save costs associated with laying new cabling intended exclusively for the operation of the security fiber-optic sensor. The effort to save

on optical fibers led to the army's requirement that the sensor use only one single optical fiber or, alternatively, a dense wave multiplex.

All input requirements of the army had to be included in the research as the army is the intended end-user. In addition, the requirements of companies in the petrochemical and biomedical engineering industries were also applied. This sensor can cover the need for high-quality non-electrical sensors in refineries and medical applications. The previous research and experience in the University of Defense laboratories have shown that these requirements can be tested in a laboratory. It has been shown that when powering optical fiber polarization sensors, polarization multiplexes can also be used, thereby saving even more transmission bandwidth and, thus, financial costs [3]. It has also been demonstrated that it is possible to use special elements such as depolarizers, double sensors [4], or circular polarizers [5] when supplying power over long routes. Other works have attempted to use multiplexing technology (DWDM) for powering sensors, and they describe the beginnings of research into polarization sensors for military purposes [6,7]. The mentioned research has shown that the proposed technologies are fully functional as tested in laboratory conditions and, in some cases, in real environments and real optical routes. For the real-life testing of our sensor, the Brno Experimental Academic Optical Network (BEAON) and the military training facilities in Boletice and Březina were used.

There is existing research regarding sensors that utilize ultra-low-loss dispersion-flattened polymer optical fibers [8] or the testing of sensors using fiber Bragg gratings [9]. Another significant contribution in the field is the use of erbium-doped fiber amplifiers (EDFA) [10–12], which led to the improvement of the fiber-based temperature sensor. The recent advances in high-birefringence fiber loop mirror-based sensors [13] and the research on photonic crystal fiber sensors [14] have demonstrated the possibilities of using alternative types of optical fibers. The considered type of sensor can also be used in biomedical applications [15] or as an environmental monitoring network for quantum gas experiments [16]. The periodic thermal cycling method can be used for the dynamic polarization response of polarization-maintaining fibers [17]. Solid-core anti-resonant fibers with nested circular tubes can also be developed to exhibit a polarization-maintaining performance [18]. The aforementioned research has shown that polarization fiber-optic sensors are increasingly utilized, especially for security technology in dangerous environments, while in some cases, they are supplemented or combined with fiber Bragg gratings [9]. Additional sources of information for the scientific results presented in this paper can be found in the literature [19–23], and an excellent overview of known and used sensors is described in [24]. Current measurement methods do not allow the use of polarization sensors over long distances as it is not possible to ensure the symmetrical excitation of both polarization planes. However, fiber-optic systems have superior properties compared to microwave communication. The advantages of optical fiber can thus be compared, for example, with works related to telecommunication fibers [25], and they are suitable for biomedical applications [26], nano/imaging [27], and optical nanoscopy [28].

## 2. Theoretical Basis and Methods

The general description of the new type of sensor with a circulator and polarization splitter can be divided into two parts: the circulator and the sensor, and the latter consists of the polarization splitter and the sensor fiber. The circulator introduces the optical wave into the sensor and transmits the received optical wave to the detector. The used splitter is polarization-maintaining, i.e., it transfers the polarization from the output of the source without affecting it. The sensor part itself is fundamentally influenced by the properties of the polarization splitter. The polarization-maintaining input fiber defines two polarization states, propagating in the slow and fast depolarization axes. These are separated by introducing the slow axis polarization into one direction and the fast axis polarization into the other, which it rotates by 90°. Both paths are bidirectional and remain part of the single fiber, forming a loop with the polarization-maintaining (PM) sensor. For

an optical wave entering the paths of the splitter, the inputs behave as a linear polarizer of the same orientation. This can be deduced from both the basic principle and experiments.

For the basic arrangement, the schematic representation of the sensor in Figure 1 can be used to calculate the transmission properties of the sensor. For the calculation, a coordinate system was chosen with the  $x$ -axis coinciding with the fast  $f$ -axis and the  $y$ -axis coinciding with the slow  $s$ -axis. This is the usual marking when describing a retarder using the Jones matrix.

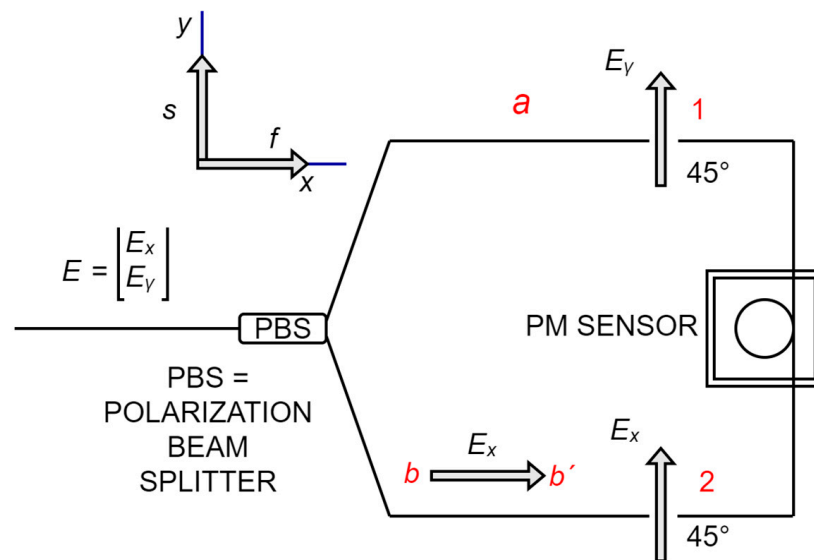


**Figure 1.** Basic arrangement of the sensor—a schematic overview. Notes 1 and 2 refer to the direction of light propagation (1→2) or (2→1).

The areas where the individual components of the sensor come into contact are marked in red in the figure and are used for orientation purposes during the calculation. The optical wave at the input of the splitter, generally of any polarization, is split into two orthogonal components into paths  $a$  and  $b$ . Both paths  $a$  (1→2) and  $b$  (2→1) can be roughly described using the symbols marked in red and schematically represented by block diagrams. The descriptions given in Figures 2 and 3 apply to the arrangement of both paths. The 90° symbol for the polarizer and rotator denotes a 90° rotation from the  $x$ -axis, i.e., to the  $y$ -axis.

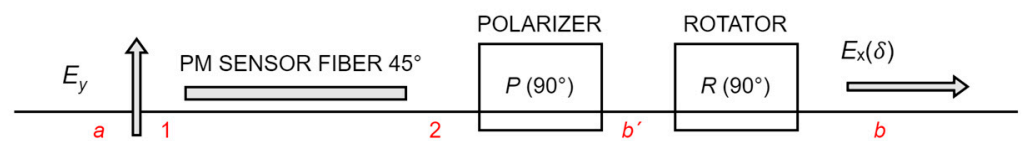


**Figure 2.** Arrangement of path  $a$ :  $a \rightarrow 1 \rightarrow 2 \rightarrow b' \rightarrow b$ .

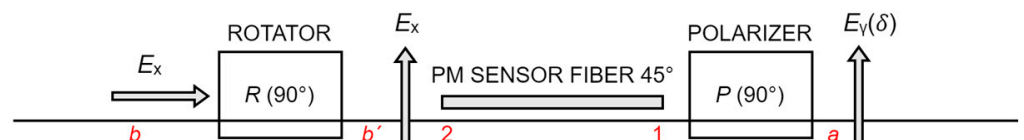


**Figure 3.** Arrangement of path  $b$ :  $b \rightarrow b' \rightarrow 2 \rightarrow 1 \rightarrow a$ .

To calculate the response of the sensor, it is necessary to compile a chain of Jones matrices describing the passage of the optical wave through both paths [5]. A prerequisite for the use of Jones matrices is the full polarization of optical waves, which we assumed

was met in this model case. At the input of the splitter is an optical wave, which is described by the Jones vector as follows:

$$E = \begin{bmatrix} E_x \\ E_y \end{bmatrix} \quad (1)$$

with the intensity

$$I_{in} = E_x E_x^* + E_y E_y^* \quad (2)$$

For path *a*, the following applies:

$$R(90)P(90)L(45) \begin{bmatrix} 0 \\ E_y \end{bmatrix} = \begin{bmatrix} 0 & 1 \\ -1 & 0 \end{bmatrix} \begin{bmatrix} 0 & 0 \\ 0 & 1 \end{bmatrix} \begin{bmatrix} \cos \frac{\delta}{2} & i \sin \frac{\delta}{2} \\ i \sin \frac{\delta}{2} & \cos \frac{\delta}{2} \end{bmatrix} \begin{bmatrix} 0 \\ E_y \end{bmatrix} = \begin{bmatrix} E_y \cos \frac{\delta}{2} \\ 0 \end{bmatrix} \quad (3)$$

For path *b*, the following applies:

$$P(90)L(45)R(90) \begin{bmatrix} E_x \\ 0 \end{bmatrix} = \begin{bmatrix} 0 & 0 \\ 0 & 1 \end{bmatrix} \begin{bmatrix} \cos \frac{\delta}{2} & i \sin \frac{\delta}{2} \\ i \sin \frac{\delta}{2} & \cos \frac{\delta}{2} \end{bmatrix} \begin{bmatrix} 0 & 1 \\ -1 & 0 \end{bmatrix} \begin{bmatrix} 0 \\ -E_x \end{bmatrix} = \begin{bmatrix} 0 \\ -E_x \cos \frac{\delta}{2} \end{bmatrix} \quad (4)$$

In the shared part of both paths (the common fiber), the two polarization components will merge, as follows:

$$E_{out} = \begin{bmatrix} E_y \cos \frac{\delta}{2} \\ -E_x \cos \frac{\delta}{2} \end{bmatrix} = \cos \frac{\delta}{2} \begin{bmatrix} E_y \\ -E_x \end{bmatrix} \quad (5)$$

It follows from the relation that the output optical wave is orthogonal to the input optical wave. The resulting intensity  $I_{out}$  is:

$$I_{out} = \cos^2 \frac{\delta}{2} (E_y E_y^* + E_x E_x^*) = \frac{1}{2} (1 + \cos \delta) I_{in} \quad (6)$$

From Equation (6), it follows that the output intensity is equal to the input intensity, which is modulated by the cosine function of the phase shift  $\delta$ , which changes with the temperature of the fiber.

### 3. Experimental Results

To verify the results of the calculations and the initial laboratory tests, it was necessary to experimentally verify the dependence of the phase (power at the circulator output) on thermal exposure. Subsequently, we verified the state of polarization at the sensor output, which should not have changed. A separate measurement was completed for this verification, independent of the phase dependence measurement. Finally, it was necessary to include a device for changing the polarization (a polarization controller) in the route between the circulator and the sensor and to expose the sensor to heat. In this way, it was possible to experimentally determine what happened to the polarization state during the various changes in the input polarization.

The connection with the circulator is shown in Figure 4. The light source was a standard small form-factor pluggable (SFP) module (army requirement). Due to the circulator, a single fiber was used to introduce the optical wave into the sensor fiber, which was located in a hazardous environment, and carry the phase-modulated optical wave from the sensor fiber to the detector.

A long supply route (in the order of kilometers) is typical for this connection, and only the non-electrical sensor and splitter needed to be placed in a hazardous environment. The polarization splitter is a device used to separate the fast axis from the slow axis and excite both ends of the sensor in opposite directions, as indicated by the theoretical assumptions of this experiment. In these experiments, a polarization-independent circulator (P/N: CIRC-SM-55-FC-ABS-1m-d2mm), a splitter (P/N: PBC-1X2-P-1550-900-3-1-FC), and PANDA-type, fiber-type sensors with lengths of 4 m were used. The thermal excitation was created using crushed ice at a temperature of 0 °C. The total measurement time was

920 s, and the ice was applied at 140 s. The ambient temperature was 24 °C. The measured values are shown in Figure 5.

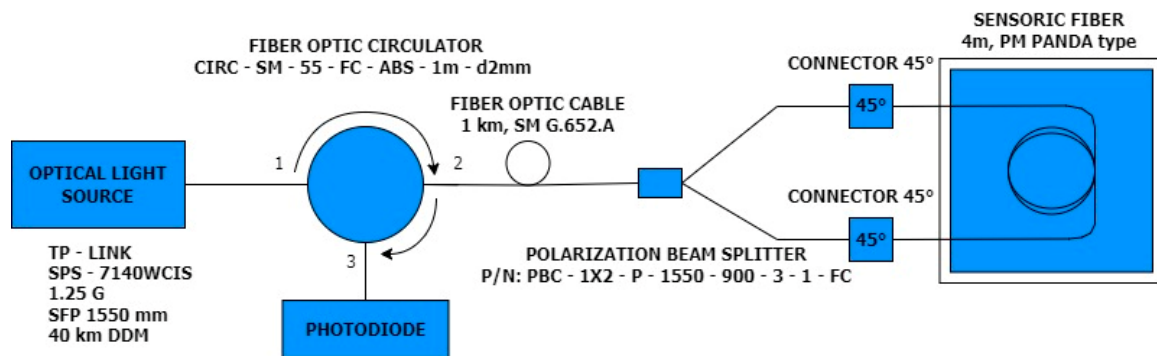


Figure 4. Wiring diagram with the circulator and two-way sensor (measurement no. 0379).

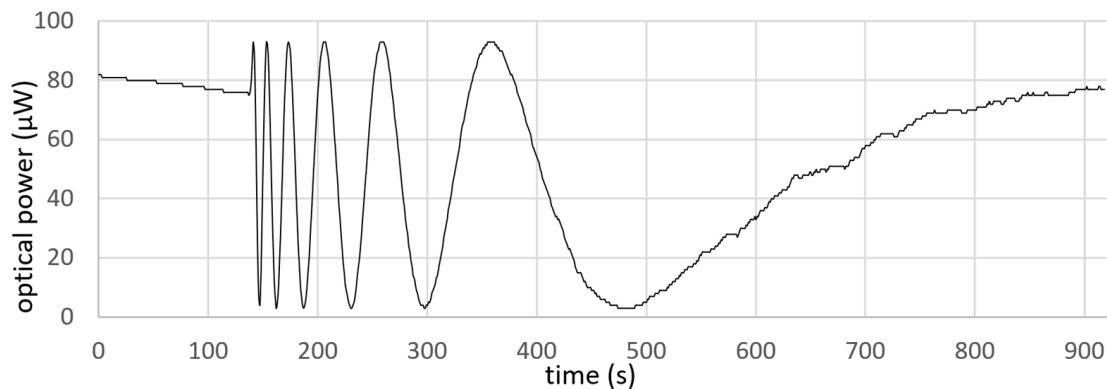
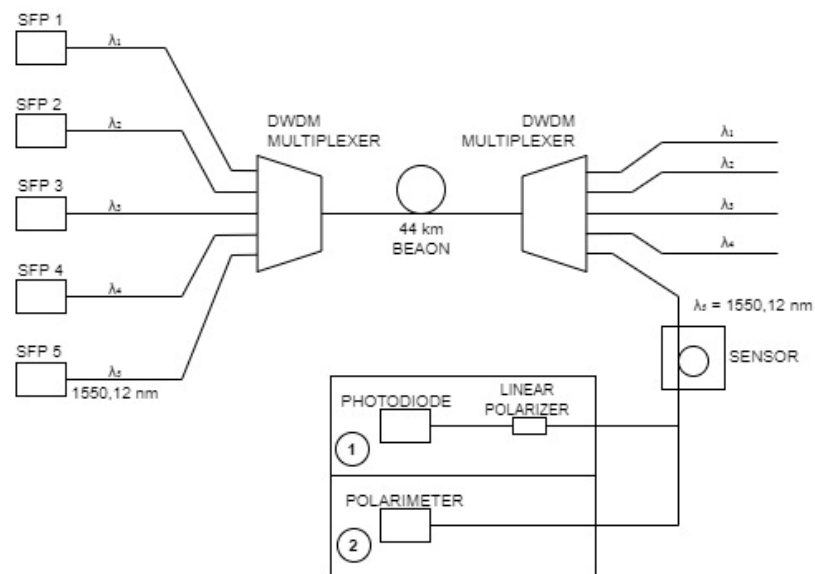


Figure 5. The intensity of the optical signal detected by the photodiode (measurement 379) using a basic connection with a circulator and an optical route with a length of 1 km, according to Figure 4.

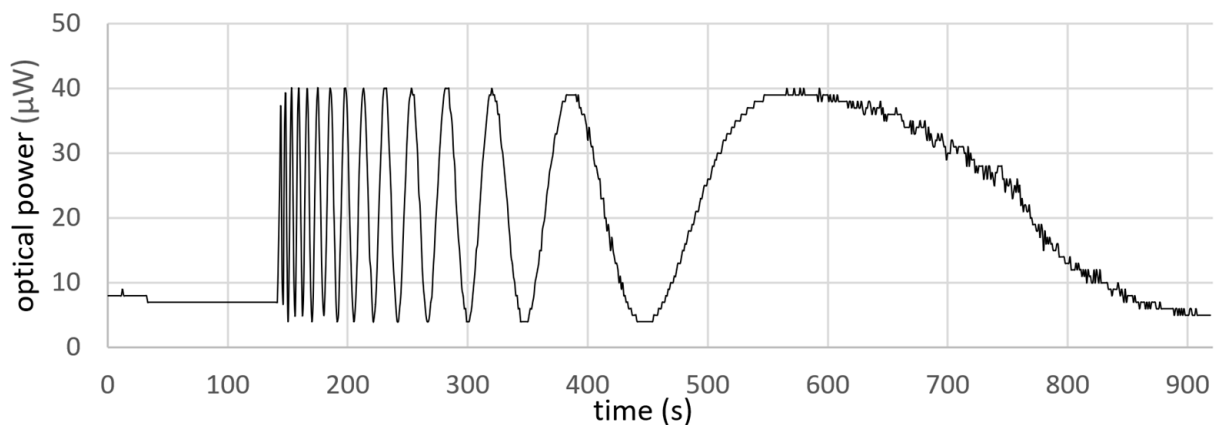
In parallel, the workplace for the cascade of polarization-maintaining sensors in the 50 GHz DWDM grid was prepared. Emphasis was placed on the use of light sources typically used in telecommunication technology, and professional sources of coherent radiation were completely abandoned. Although sources of the CLD1015 series (Thorlabs) served well for laboratory measurements [6,7], the researchers were aware that for practical use in existing telecommunication networks, common telecommunication signal sources of the SFP (small form-factor pluggable) port-type were more suitable. A TP LINK MC220L media converter with a DWDM-120-1Gbps SFP port on channel nos. 27, 29, 31, and 33 in the 50 GHz grid was used as a signal source.

The main purpose of dividing the measurements into stages and gradually connecting the channels was to demonstrate that a dense wave multiplex is not an obstacle for powering polarization fiber-optic sensors. Preparatory work and individual preparations were therefore realized with the knowledge that the polarization state of the light can change arbitrarily, which is due to the nature of the long SM cables used. Individual preparations were therefore solved in several variants. Although all measurements showed sufficient sensitivity in the laboratory environment, complications were expected when measuring on the Brno academic network, especially regarding the sensitivity of the measuring apparatus. The connection of the test route is shown in Figure 6, and the optical route was replaced by a real route between the University of Defense and The University Hospital Brno. The sensor was placed within the hospital premises to meet the requirements of the intended biomedical environment.



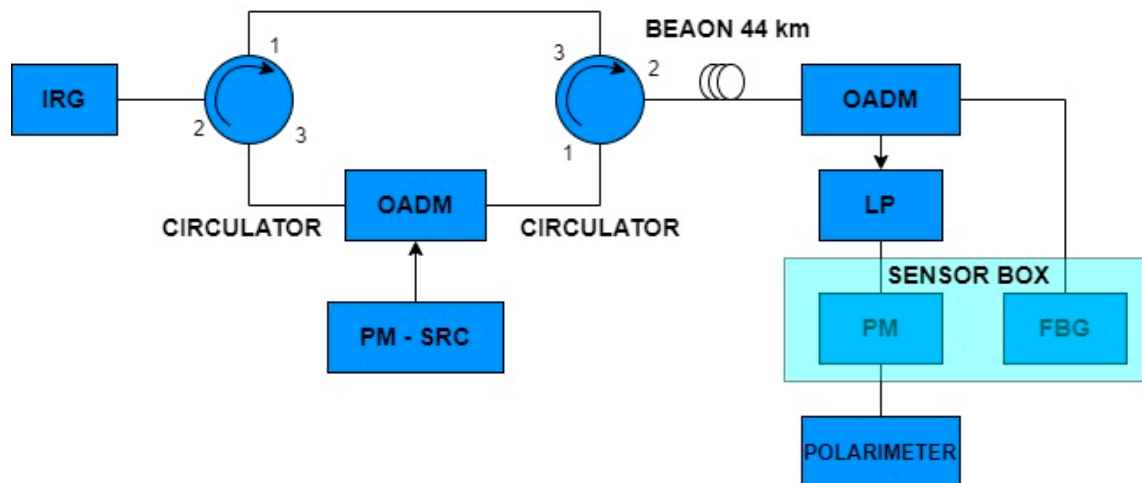
**Figure 6.** Arrangement for the measurements of the polarization properties of the passive DWDM systems. BEAON—Brno Experimental Academic Optical Network (the University of Defense to The University Hospital Brno to the Brno University of Technology). (1) and (2) are methods of measurement (Photodiode or Polarimeter).

Figure 7 depicts changes in the optical power on the photodiode of the evaluation electronics [29]. The route from the source to the sensor was a total of 44 km long (optical route: the University of Defense to The University Hospital Brno to the Brno University of Technology) and included the DWDM multiplex that we implemented. Following the sensor, there was another 5 km of optical fiber to take the signal to a safe area, terminating in the detector. In practice, however, we did not expect such significant lengths of optical cable on the input and output routes. This was a model case to determine whether the amount of optical power would be sufficient for the evaluation electronics. For the measurements, we utilized an assembled sensor (two-fiber) [6], an exposure length of 4 m, a linear polarizer, and a photodiode at the input of the measuring electronics [25]. The temperature source (the crushed ice with a temperature of 0 °C) was applied at 140 s. The total length of the measurement was 920 s. If we compare Figures 5 and 7, the difference in sensor sensitivity is noticeable. The arrangement according to Figure 6 does not allow for a connection with a circulator, which is why a two-fiber assembled sensor [6] was used.



**Figure 7.** Changes in light power (μW) in time (s) as detected by the assembled sensor at 1550 nm, with measurements performed using a photodiode (DWDM (44 plus 5 km)) and an exposure temperature of 0 °C (a measurement of 355 s).

Nearly identical results were achieved during the control measurements with the Fiber Bragg Gratings (FBGs). The PM sensors responded very well to rapid changes in the monitored physical quantity, e.g., the temperature. Slow changes, on the other hand, could be easily filtered out. FBGs are very suitable for monitoring slow events, but unfortunately, they are unsuitable for monitoring fast changes due to the design of the interrogator. The measurement was compared with other works utilizing a similar sensor principle using FBGs [9]. The connection is shown in Figure 8, and the optical route was, again, the Brno Experimental Academic Optical Network (BEAON). A single fiber sensor was used for simplicity [6].



**Figure 8.** Basic wiring of a combined sensor that uses a single-fiber polarization sensor, FBGs, and DWDM technology. IRG—interrogator, BEAON—Brno Experimental Academic Optical Network, LP—linear polarizer, OADM—optical add-drop multiplexer.

An FBG generally requires a spectrally wider transmission channel than a PM sensor. Therefore, we connected the interrogator to the assembly using a circulator, which further split the incoming and outgoing directions. We used an OADM multiplexer to separate the signals and bring the rest of the spectrum to an FBG. The sensors (PM and FBG) were placed in a polystyrene box and exposed to thermal radiation. The recording of the measurement of the change in temperature caused by the application of crushed ice is shown in Figure 9.

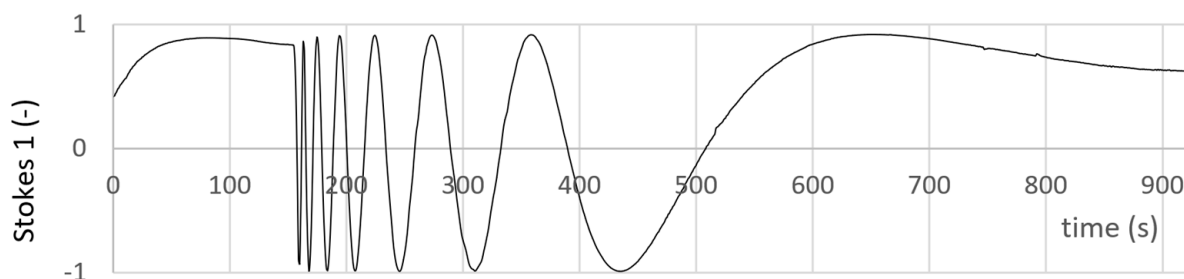


**Figure 9.** Changes in the Stokes parameter  $S_1$ : changes in the polarization state occurred when connecting a single-fiber polarization sensor [6], FBGs, and DWDM technology (a measurement of 364 s).

The biggest challenge was to design a sensor that was powered over long distances. If we assumed that only the passive component could be placed inside dangerous and restricted areas, it was necessary to calculate the attenuation of the route twice. For routes with lengths of tens of kilometers, the amount of useful signal may no longer have been sufficient, which was why it was necessary to use amplifiers. An EDFA amplifier (Keopsys

KPS-BT2-C-10-LN-SA) with a maximum (saturated) output power of +15 dBm and a maximum gain of 15 dB was used for the control measurements. The gain was set by directly adjusting the pump diode current.

During the measurement, the pump diode current was set to 80 mA and the corresponding optical power level was 12.7 dB. The signal level at the input to the EDFA was  $-5.9$  dBm and the output power was  $+6.8$  dBm. A circuit diagram with the EDFA amplifier is shown in Figure 10.

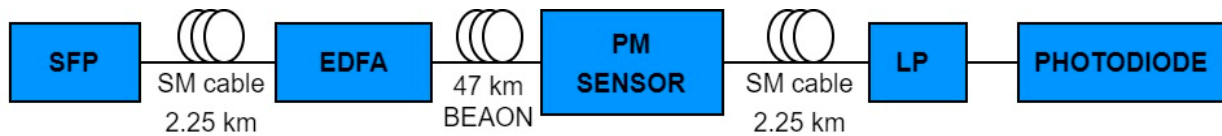


**Figure 10.** Simplified connection of the PM sensor measurement on the amplified optical path (EDFA). SFP—light source, EDFA—amplifier, LP—linear polarizer, BEAON—Brno Experimental Academic Optical Network.

The experimental laboratory measurements were followed by measurements on a real route (the BEAON). In this case, the pump diode current was set to a limit value of  $-156$  mA. The output power of the EDFA was  $+10.7$  dBm. The sensor output signal captured on the VEGA optical power meter is shown in Figure 11. It is evident from the shape of the graph that we were already approaching the limit of the detector's distinguishing capabilities.

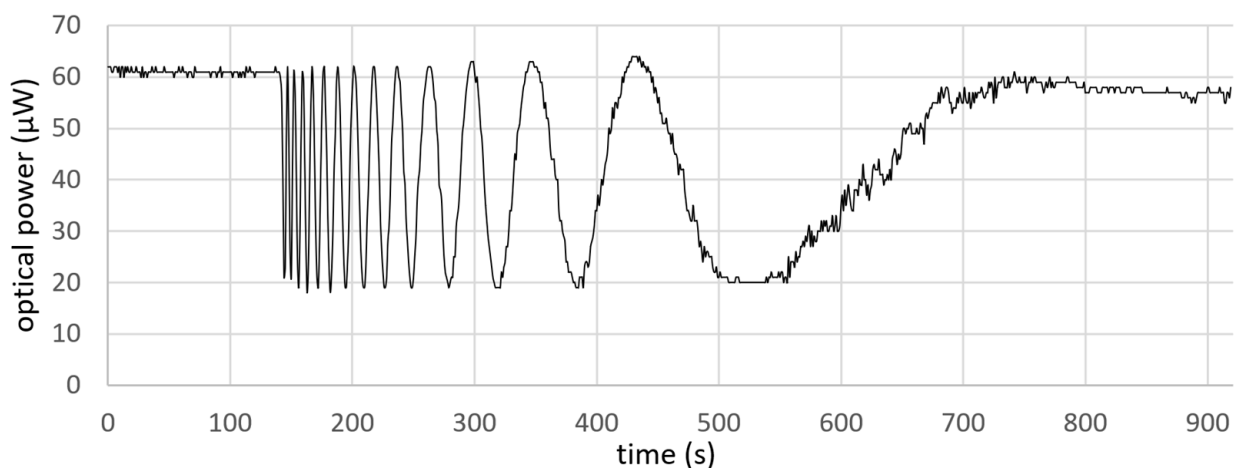


**Figure 11.** Simplified connection of the PM sensor measurement on the amplified optical path (EDFA). SFP—light source, EDFA—amplifier, LP—linear polarizer, BEAON—Brno Experimental Academic Optical Network.

It can be seen in Figure 11 that the performance did not drop to zero (or close to zero), as in the previous cases. This was due to the considerable performance of the EDFA amplifier, the increasing problems with reflections and dispersions, and, thus, the decreasing proportion of polarized light. In addition, the degree of polarization in front of the linear polarizer fluctuated [4], and thus, power was lost (approximately  $20$   $\mu$ W), which could not be used, and thus, it caused a decrease in sensitivity. When amplifying the useful EDFA signal by an amplifier, it is difficult to use a connection with a circulator (Figure 4). This is due to a parameter called channel cross-talk between ports 1 and 3. At lengths greater than approximately 30 km, the amount of uninfluenced light begins to increase disproportionately, and the amplifier does not have the desired effect. The only correct solution appears to be the use of two separate fibers (Figure 10). All described measurements on the Brno Experimental Academic Optical Network (BEAON) showed excellent results. The specific method of measurement must be chosen with regard to the application under consideration. By comparing Figures 9 and 11, we can see a noticeable difference in the sensor sensitivities.

In the measurement according to Figure 10, a single-fiber sensor [6] was used, and in the connection according to Figure 11, a two-fiber assembled sensor [6] was used.

In the mentioned cases, the optical power changes (Figure 5, 7 and 11), which characterized the course of the phase, changed over time. The optical power range from minimum to maximum corresponded to the phase change  $\pi$ . The range of change in the Stokes parameter in Figure 9 corresponded to the change in phase  $2\pi$ . From there, it was possible to determine the dependence of the phase on time ( $\varphi(t)$ ) for a specific arrangement of the sensor. From this, the corresponding sensitivity per unit length was  $\frac{1}{l} \frac{\Delta\varphi}{\Delta t}$ , where  $l$  is the length of the fiber and the phase change is  $\Delta\varphi$  for the time  $\Delta t$ . Instant sensitivity can be determined for individual cases according to the following methodology:

$$\text{norm.SENSITIVITY} = \frac{n \cdot 2\pi}{t \cdot l}, \quad (7)$$

where  $n$  is the number of orbits along the Poincaré sphere (or complete waveforms for power changes),  $t$  is the time, and  $l$  is the length of the exposed sensory section.

The specific sensitivity of our sensor was, therefore,  $4 \text{ rad} \cdot \text{s}^{-1} \cdot \text{m}^{-1}$ . However, this sensitivity only applied to the chosen configuration of the sensor in space and was difficult to generalize. In addition, the sensitivity depended on other variables, especially meteorological conditions, provided the measurement was carried out in an outdoor environment.

The most valuable practical experiments were performed in the military areas of the Army of the Czech Republic. The Boletice Military Training Area (Pražačka Artillery Pit) was used to measure detonations of trinitrotoluene (TNT—IUPAC 2-methyl-1,3,5-trinitrobenzene) organic explosives. The measurements were performed with a 200 g bomb of TNT and took place in March of 2022. Subsequently, measurements were made for charges weighing from 5 to 15 kg of TNT. An example of the TNT installation for the measurements is shown in Figure 12, along with the installation of the fiber-optic sensor and supply cabling. The measuring fibers were placed at different distances and in different orientations towards the explosions. During the entire measurement period, the measuring electronics [25] were located in the bunker and the input optical fibers were 1 km long.



**Figure 12.** Installation of a TNT charge and an optical fiber sensor for measuring 5 kg of TNT (Boletice Military Training Area, Pražačka Artillery Pit).

A similar measurement was carried out in the Březina Military Training Area in October of 2022. This area is not equipped with an artillery pit, and therefore, mainly the effects of the movement of people in closed buildings and outdoor spaces were tested. An example of the installation can be seen in Figure 13.



**Figure 13.** Installation of the polarization sensor and supply cabling in the Březina military area.

It was clear from the results obtained in the military areas that the polarization sensors using DWDM technology, in particular, were very suitable for this type of measurement. The choice of sensor type (single, two-fiber assembled, or two-way single fiber) depends on the specific application. Figure 14 shows the response to an explosion at a distance of 100 m from the sensing PM fiber for one of the possible arrangements of a single-fiber sensor. High speed and low capacitance in a direct fiber-coupled FC/PC package (Thorlabs FGA01FC) were used for the evaluation. Due to the spatial orientation and location of the sensor, the result was a record of the surge wave of the measured detonation (15 kg of TNT).

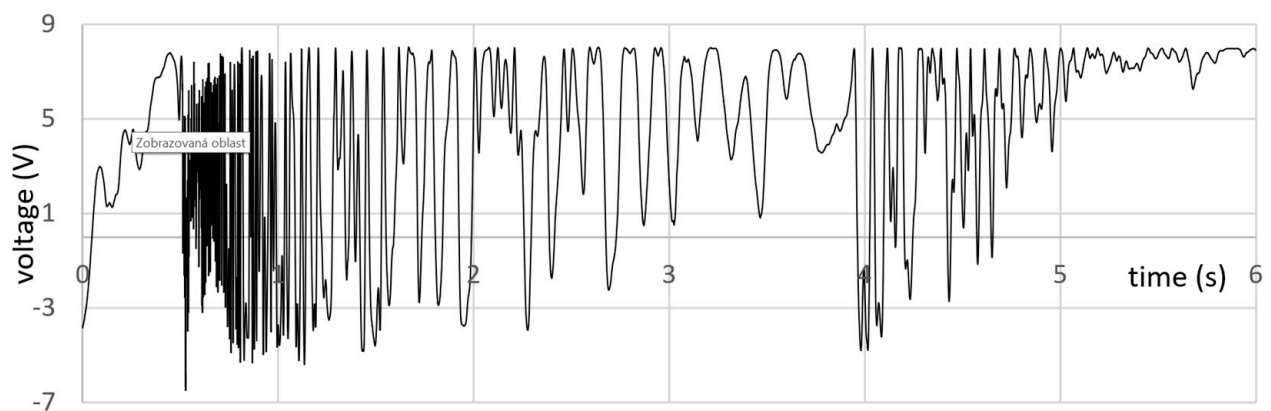


**Figure 14.** Detonation measurement for 15 kg of TNT at a distance of 100 m from the sensing PM fiber (4 m, single-fiber-type, transverse placement, tensioned, and a supply cable of 300 m in length). Graph of the dependence of the output voltage on time showing the effect of the surge wave (a measurement of M2-6-A).

The experiment was conducted as a guide in order to assess the suitability of the sensor arrangement for the given application. The sensor fiber responded to a shock wave, consisting of both a pressure wave and a thermal wave (see Figure 14). This resulted in the need for further investigations in defined, laboratory conditions that can simulate both components of the shock wave. It will also be necessary to search for suitable arrangements of the sensor fiber in the sensor to achieve the maximum response.

#### 4. Discussion

It was shown that the function of the circulator sensor is not affected by the input polarization state, which can be arbitrary due to the type of connection. The arrangement practically corresponds to a two-fiber arrangement, except that the two sensor fibers were replaced by one in which the optical waves propagated in opposite directions.

When we excited the sensor with linear polarization only in the slow axis, the sensor fiber was excited only in one direction. Due to various changes in the polarization state, the sensitivity of the sensor was constant over time and did not fluctuate as it did with other sensor types. The output signal was the intensity of the input optical wave, modulated by the cosine function of the phase shift, which depended on the continuous temperature of the fiber. Due to the fact that no specific or stable polarization state was defined, an SM fiber (cable) carrying the optical wave from the circulator to the sensor could be inserted between the circulator and the sensor. Table 1 contains an overview of the advantages and disadvantages of individual arrangements and specific applications of each arrangement.

**Table 1.** Overview of the advantages and disadvantages of individual layouts and specific applications.

Type of Sensor	Description and Properties	Applications
One-way	Simple and cheap, easy assembly, and high sensitivity; suitable for closed spaces and utilizes short supply cables/PM fibers; cannot be used with EDFA amplifiers or DWDM technology	Military facilities, warehouses, closed spaces, and local biomedical applications; unsuitable for the petrochemical industry
Two-fiber	Robust arrangement enabling remote power supply (polarization-state-independent system), possibility of combining EDFA amplifiers and DWDM technology; excellent sensitivity even in outdoor areas; necessary use of two optical fibers for the input and output of the useful signal	Military buildings, warehouses, open and closed spaces, biomedical applications, and the petrochemical industry
Circulator	Robust arrangement enabling remote power supply (polarization-state-independent system), and the use of DWDM technology is possible, but the signal cannot be amplified (EDFA); excellent sensitivity even in outdoor areas; a single optical fiber is enough to feed and remove the useful signal	Military buildings, warehouses, open and closed spaces, biomedical applications, and the petrochemical industry; wherever a single optical fiber is available

The DWDM measurements on the BEAON route in Brno unequivocally demonstrated that the type of sensor arrangement must depend on the required application as each sensor type has specific advantages and disadvantages. Furthermore, changes in the polarization state over time were practically not manifested. The measurements confirmed that the path of the optical cables on the BEAON route was not suspended in the air, but rather, it was laid in the ground along the entire length of the path. This eliminated the presence of parasitic phenomena during the detection of a disturbance in the thermal field of the sensor. However, even if a part of the path was led by suspension cables or the

polarization state of the light in the fiber was otherwise changed, our innovative connection would be able to compensate, and thus, it would have no effect on the sensitivity of the sensor. The BEAON was used over a total length of 44 km, and for each measurement, the wiring was chosen to consider the transference of the optical signal to a detector outside the potentially hazardous environment. From the figures, it is evident that the sensor reacted to temperature changes in an excellent way. In addition, due to the innovative arrangement, all negative phenomena introduced into the measuring apparatus by the used DWDM technology and dense traffic on the surrounding channels in the 50 GHz grid were eliminated. Besides these benefits, excellent sensitivity was retained over a total distance of 49 km (the BEAON plus 5 km route).

## 5. Conclusions

The polarization fiber-optic sensor arrangement has been optimized to use only a single bidirectional (two-way) optical fiber. The innovative arrangement of the sensor was tested in combinations with long power paths, DWDM technology, and EDFA amplifiers. The result of the development was a single-fiber sensor that reliably solves the problem of fluctuating polarization states. This sensor can thus be used advantageously in dangerous environments, such as military areas, ammunition warehouses, areas with a risk of explosion (ex-proof), petrochemical industrial facilities, or oil and natural gas processing equipment. It is also possible to implement the sensor in biomedical devices, where the possible electrical potential of common electronic sensors could be a complication. The long-term work of the entire research team finally fulfilled the requirement of the Czech Army for the use of a single fiber. Additionally, a version of the sensor using a dense wave multiplex DWDM was developed.

**Author Contributions:** Formal analysis, D.G.; Writing—original draft, M.K.; Writing—review & editing, J.V., K.S. and L.H. All authors have read and agreed to the published version of the manuscript.

**Funding:** This work was supported by the MVČR VI3VS/678 Instant Signal Processing Using Hybrid Systems in Defence Infrastructure project and by the institutional support of the Ministry of Defence of the Czech Republic (VAROPS).

**Data Availability Statement:** Not applicable.

**Conflicts of Interest:** The authors declare no conflict of interest.

## References

1. Zhang, F.; Lit, J. Temperature and Strain Sensitivity Measurements of High-Birefringent Polarization-Maintaining Fibers. *Phys. Comput. Sci. Fac. Publ.* **1993**, *32*, 24. [[CrossRef](#)]
2. Domanski, A. Polarization degree fading during propagation of partially coherent light through retarder. *Opto-Electron. Rev.* **2004**, *13*, 171–176.
3. Vylezich, Z.; Kyselak, M. Utilization of telecommunication optical routes to power fiber-optic polarization sensors. *Opt. Appl.* **2022**, *52*, 4. [[CrossRef](#)]
4. Kyselak, M.; Vylezich, Z.; Vavra, J.; Grenar, D.; Slavicek, K. The long fiber optic paths to power the thermal field disturbance sensor. In Proceedings of the SPIE 11682 Optical Components and Materials XVIII, Online Only, 5 March 2021; p. 116821A. [[CrossRef](#)]
5. Kyselak, M.; Grenar, D.; Slavicek, K.; Vylezich, Z.; Vavra, J. Polarizing fiber temperature sensor powered remotely by circularly polarized light. In Proceedings of the 2022 SBFoton International Optics and Photonics Conference (SBFoton IOPC), Recife, Brazil, 13–15 October 2022; IEEE: New York, NY, USA, 2022; pp. 1–4, ISBN 978-1-6654-5273-1. [[CrossRef](#)]
6. Kyselak, M.; Vavra, J.; Slavicek, K.; Grenar, D.; Bohrn, M. Fiber optic polarization temperature sensor for biomedical and military security systems. In Proceedings of the SPIE—The International Society for Optical Engineering, Orlando, FL, USA, 8 June 2022; Cullum, B.M., Ed.; SPIE: Washington, DC, USA, 2022; ISSN 0277-786X, ISBN 978-1-5106-5122-7. [[CrossRef](#)]
7. Kyselak, M.; Grenar, D.; Slavicek, K. Optical Communication Fibers Used for Security Sensors Powering. In *Lecture Notes in Networks and Systems*; Rocha, A., Ed.; Springer Science and Business Media Deutschland GmbH: San Carlos, Republic of Costa Rica, 2022; ISSN 2367-3370, ISBN 978-3-030-96292-0. [[CrossRef](#)]
8. Luo, W.; Jiang, P.; Xu, Q.; Cao, L.; Jones, A.; Li, K.; Copner, N.; Gong, Y. Terahertz Sensor via Ultralow-Loss Dispersion-Flattened Polymer Optical Fiber: Design and Analysis. *Materials* **2021**, *14*, 4921. [[CrossRef](#)]

9. Matuck, L.; Pinto, J.L.; Marques, C.; Nascimento, M. Simultaneous Strain and Temperature Discrimination in 18650 Li-ion Batteries Using Polarization-Maintaining Fiber Bragg Gratings. *Batteries* **2022**, *8*, 233. [[CrossRef](#)]
10. Li, D.; Feng, T.; Sun, W.; Wu, S.; Yan, F.; Li, Q.; Yao, X.S. Eight-Wavelength-Switchable Narrow Linewidth Erbium-Doped Fiber Laser Based on Cascaded Superimposed High-Birefringence Fiber Bragg Grating. *Electronics* **2022**, *11*, 3688. [[CrossRef](#)]
11. Cheng, D.; Yan, F.; Feng, T.; Zhang, L.; Han, W.; Qin, Q.; Li, T.; Bai, Z.; Yang, D.; Guo, Y.; et al. Six-Wavelength-Switchable SLM Thulium-Doped Fiber Laser Enabled by Sampled FBGs and  $3 \times 3$  Coupler Based Dual-Ring Compound Cavity Filter. *IEEE Photonics J.* **2022**, *14*, 1515908. [[CrossRef](#)]
12. Zhang, L.; Yan, F.; Feng, T.; Han, W.; Guan, B.; Qin, Q.; Guo, Y.; Wang, W.; Bai, Z.; Zhou, H.; et al. Six-wavelength-switchable narrow-linewidth thulium-doped fiber laser with polarization-maintaining sampled fiber Bragg grating. *Opt. Laser Technol.* **2021**, *136*, 106788. [[CrossRef](#)]
13. Frazão, O.; Baptista, J.; Santos, J. Recent advances in high-birefringence fiber loop mirror sensors. *Sensors* **2007**, *7*, 2970–2983. [[CrossRef](#)]
14. Rana, S.; Kandadai, N.; Subbaraman, H. A Highly Sensitive, Polarization Maintaining Photonic Crystal Fiber Sensor Operating in the THz Regime. *Photonics* **2018**, *5*, 40. [[CrossRef](#)]
15. He, C.; He, H.; Chang, J.; Chen, B.; Ma, H.; Booth, M.J. Polarisation optics for biomedical and clinical applications: A review. *Light Sci. Appl.* **2021**, *10*, 194. [[CrossRef](#)] [[PubMed](#)]
16. Barrett, T.; Evans, W.; Gadge, A.; Bhumbra, S.; Slegers, S.; Shah, R.; Fekete, J.; Orucevic, F.; Kruger, P. An Environmental Monitoring Network for Quantum Gas Experiments and Devices. *Quantum Sci. Technol.* **2021**, *7*, 025001. [[CrossRef](#)]
17. Hwang, S.; Lee, S.; Baek, J.; Jeong, J.; Lee, M.H.; Moon, G. Dynamic polarization response of polarization-maintaining fibers by periodic thermal cycling method. *Rev. Sci. Instrum.* **2022**, *93*, 083201. [[CrossRef](#)]
18. Zhang, S.; Sun, S.; Sheng, Q.; Shi, W.; Yan, Z.; Hao Tian, Z.; Yao, J. Polarization-Maintaining Performance of Solid-Core Anti-Resonant Fiber With Nested Circular Tubes in  $3 \mu\text{m}$  Wavelength. *J. Light. Technol.* **2022**, *40*, 1137–1143. [[CrossRef](#)]
19. Spurny, V.; Munster, P.; Tomasov, A.; Horvath, T.; Skaljo, E. Physical Layer Components Security Risks in Optical Fiber Infrastructures. *Sensors* **2022**, *22*, 588. [[CrossRef](#)]
20. Abbas, H.S.; Gregory, M. The next generation of passive optical networks A review. *J. Netw. Comput. Appl.* **2016**, *67*, 53–74. [[CrossRef](#)]
21. Koudelka, P.; Siska, P.; Latal, J.; Poboril, R.; Hajek, L.; Kepak, S.; Vasinek, V. Security risk assessment of the primary layer of wavelength division multiplexing passive optical network. In Proceedings of the SPIE 9450, Photonics, Devices, and Systems, Prague, Czech Republic, 27–29 August 2015; Volume 6. [[CrossRef](#)]
22. Diao, M.; Shalaby, M.; Mohamed, A.A.; Hassan, K.M.M.; Mokhtar, A.M. Undetectable Tapping Methods for Gigabit Passive Optical Network (GPON). In Proceedings of the 14th International Computer Engineering Conference (ICENCO), Cairo, Egypt, 29–30 December 2018; pp. 52–57. [[CrossRef](#)]
23. Fok, M.P.; Wang, Z.; Deng, Y.; Prucnal, P. Optical Layer Security in Fiber-Optic Networks. *IEEE Trans. Inf. Forensics Secur.* **2011**, *6*, 725–736. [[CrossRef](#)]
24. Pendão, C.; Silva, I. Optical Fiber Sensors and Sensing Networks: Overview of the Main Principles and Applications. *Sensors* **2022**, *22*, 7554. [[CrossRef](#)] [[PubMed](#)]
25. Agrell, E.; Karlsson, M.; Chraplyvy, A.R.; Richardson, D.J.; Krummrich, P.M.; Winzer, P.; Roberts, K.; Fischer, J.K.; Savory, S.J.; Eggleton, B.J.; et al. Roadmap of optical communications. *J. Opt.* **2016**, *18*, 6. [[CrossRef](#)]
26. Chin, A.L.; Jiang, S.; Jang, E.; Niu, L.; Li, L.; Jia, X.; Tong, R. Implantable optical fibers for immunotherapeutics delivery and tumor impedance measurement. *Nat. Commun.* **2021**, *12*, 5138. [[CrossRef](#)] [[PubMed](#)]
27. Ma, X.; Liu, Q.; Yu, N.; Xu, D.; Kim, S.; Liu, Z.; Jiang, K.; Wong, B.M.; Yan, R.; Liu, M. 6 nm super-resolution optical transmission and scattering spectroscopic imaging of carbon nanotubes using a nanometer-scale white light source. *Nat. Commun.* **2021**, *12*, 6868. [[CrossRef](#)] [[PubMed](#)]
28. Kim, S.; Yu, N.; Ma, X.; Zhu, Y.; Liu, Q.; Liu, M.; Yan, R. High external-efficiency nanofocusing for lens-free near-field optical nanoscopy. *Nat. Photonics* **2019**, *13*, 636–643. [[CrossRef](#)]
29. Vavra, J.; Kyselak, M. Analog Signal Processing for Fiber Optic Sensor Detecting Temperature Changes. In Proceedings of the 2020 27th International Conference on Telecommunications (ICT), Bali, Indonesia, 5–7 October 2020; IEEE: New York, NY, USA, 2020; ISBN 978-1-7281-6587-5. [[CrossRef](#)]

**Disclaimer/Publisher’s Note:** The statements, opinions and data contained in all publications are solely those of the individual author(s) and contributor(s) and not of MDPI and/or the editor(s). MDPI and/or the editor(s) disclaim responsibility for any injury to people or property resulting from any ideas, methods, instructions or products referred to in the content.